Magnetic, transport and thermal properties of ternary indides R_2CoIn_8 (R = rare earths and Y)

2007 J. Phys.: Condens. Matter 19 136216

(http://iopscience.iop.org/0953-8984/19/13/136216)

IOP PUBLISHING JOURNAL OF PHYSICS: CONDENSED MATTER

J. Phys.: Condens. Matter **19** (2007) 136216 (26pp) doi:10.1088/0953-8984/19/13/136216

Magnetic, transport and thermal properties of ternary indides R_2CoIn_8 (R = rare earths and Y)

Devang A Joshi[1], **C V Tomy**[1] **and S K Malik**[2]

[1] Department of Physics, Indian Institute of Technology, Mumbai 400076, India
[2] (ICCMP) University of Brasilia, Brasilia, Brazil

Received 9 January 2007, in final form 13 February 2007
Published 13 March 2007
Online at stacks.iop.org/JPhysCM/19/136216

Abstract

The magnetic properties of the R_2CoIn_8 series of compounds are studied. Y_2CoIn_8 shows a Pauli paramagnetic behaviour. Ce_2CoIn_8 shows a heavy fermion and Kondo behaviour. Pr_2CoIn_8 shows a dominating crystal field effect. The compounds with other magnetic rare earths (R = Sm, Nd, Gd, Tb, Dy and Ho) show antiferromagnetic ordering at low temperatures with T_N = 12, 10, 33.5, 30, 17.4 and 7.6 K, respectively. Dy_2CoIn_8, Ho_2CoIn_8 and Nd_2CoIn_8 show metamagnetic transitions and a field-induced ferromagnetic transition at 2 K and above ≈82, 54 and 85 kOe respectively. Gd_2CoIn_8 is a strong antiferromagnet. Sm_2CoIn_8 shows a dominating antiferromagnetic behaviour with a ferromagnetic component at low temperatures. Tb_2CoIn_8 shows a ferromagnetic component at low temperatures with the possibility of superconducting behaviour below 2.5 K. The compound also shows metamagnetic transitions in the magnetic isotherm and the possibility of complicated magnetic structure below the transition temperature.

(Some figures in this article are in colour only in the electronic version)

1. Introduction

Ternary indides involving rare earths are widely studied with respect to a variety of interesting phenomena exhibited by the rare earth ions. The interesting features include heavy fermion behaviour, valence fluctuation, Kondo behaviour, various magnetic orderings, metamagnetic transitions, magnetoresistance, etc. Most of these properties arise in the rare earth compounds due to a variety of interactions involving the 4f orbital, d orbital and conduction electrons including the environmental effect of the crystal field, internal magnetic field and structure. The 4f orbital is at the centre of all the interesting physical phenomena that arise. This gives us an opportunity to explore the behaviour of 4f electrons for a variety of fundamental studies and possible practical applications.

The ternary indides R_2CoIn_8 belong to a family of compounds represented by a general formula R_nTIn_{3n+2} (R = rare earths, T = Co, Rh and Ir). Within this family $n = 1$ gives the $RTIn_5$ series of compounds and $n = 2$ gives the R_2TIn_8 series of compounds. These series of compounds were first reported by Kalychak *et al* [1, 2], who gave the results of their crystallographic studies on these compounds. The Ce compounds within this family have been studied, and their behaviour is as follows.

With T = Rh, both $n = 1$ and 2 compounds are antiferromagnetic, with Néel temperature $T_N = 3.8$ and 2.8 K respectively [3, 4]. Both compounds exhibit a superconducting state at 2 K and under a pressure of 1.6 and 2.3 GPa respectively [3, 5].

With T = Ir, $CeIrIn_5$ is a heavy fermion superconductor ($T_C = 0.4$ K) [6] and Ce_2IrIn_8 is a heavy fermion paramagnet.

With T = Co, both $CeCoIn_5$ and Ce_2CoIn_8 are heavy fermion superconductors, with $T_C = 2.3$ and 0.4 K respectively [7, 8]. Apart from this, a high-pressure transport study is reported in the case of Ce_2CoIn_8 [9]. We have reported on R_2CoIn_8 (R = Ce, Pr and Dy) compounds [10]; Dy_2CoIn_8 shows interesting magnetic properties and Pr_2CoIn_8 shows crystal field effects.

To the best of our knowledge there are no other reports on Ce_2CoIn_8 and other rare earth compounds in the same series. Considering this and a variety of interesting behaviour in this family of compounds we decided to study the R_2CoIn_8 compounds with all possible rare earths, and we now report on our detailed study of the magnetic, thermal and transport properties of these compounds.

2. Experimental details

The starting materials used for the preparation of the R_2CoIn_8 series of compounds were the high-purity metals R ($\approx$ 99.95%), Co (99.9%) and In (99.99%) from *Alfa Aeser, UK*. Stoichiometric amounts of the metals were melted in an arc furnace on a water-cooled cooper hearth under a titanium-gettered argon atmosphere. The buttons were flipped over and remelted three times to ensure the homogeneity of the compound formed. An extra 5% of indium (of the total indium weight) was added to compensate for the indium loss (due to vaporization) during melting. The buttons were then wrapped in tantalum foil, sealed in an evacuated quartz tube and annealed for 1 month at 600 °C, and then cooled slowly to room temperature. The powder x-ray diffraction patterns of all the samples were obtained on a Siemens x-ray diffractometer at room temperature, using Cu Kα radiation and pure Si as an internal standard. In order to know the effect of annealing on the formation of the compound, x-ray patterns before and after the annealing of the samples were compared. It was found that the as-melted samples do not form in a single phase. Some of the diffraction lines of the as-melted samples could be indexed to RIn_3, $CoIn_2$ and In phases. This shows that annealing causes the interdiffusion of various phases to form the R_2CoIn_8 compound. Our experiment to improve the homogeneity of the compound by annealing it at high temperature (750 °C) failed. The compound decomposed back to RIn_3 phase with other impurity phases. A small amount of indium impurity was found in some of the compounds. Er_2CoIn_8 could not be formed by this technique; three of our trials failed. A report on this series of compounds [1] says that Er forms a compound with the R_2CoIn_8 phase but not with $RCoIn_5$ phase. One of the possible reasons is that, since both series of compounds (R_2CoIn_8 and $RCoIn_5$) have the same origin, Er_2CoIn_8 might be on the border of crystallographic stability. The La-based compound does not form in any of the series.

Magnetization measurements were carried out using SQUID (superconducting quantum interference device), vibrating sample magnetometers (VSM) (Quantum Design, USA) and a VSM (Oxford Instruments). Heat capacity and resistivity measurements were performed using a physical property measurement system (PPMS) (Quantum Design, USA).

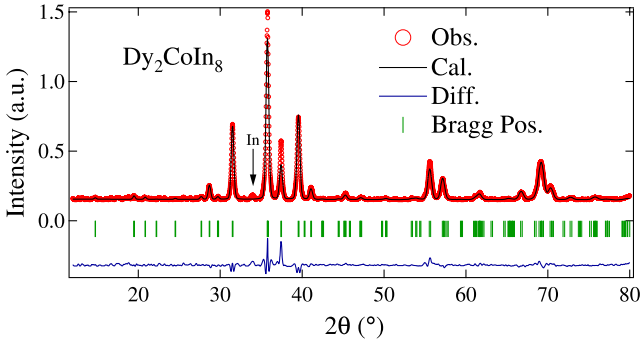

Figure 1. The observed and calculated diffraction pattern of Dy_2CoIn_8 along with the difference. The vertical bars indicate Bragg diffraction positions. The arrow indicates the In peak.

Table 1. Lattice parameters, unit cell volume and c/a ratio for the R_2CoIn_8 series of compounds.

Compound	a (Å)	c (Å)	V (Å^3)	c/a
Ce_2CoIn_8	4.64	12.251	263.759	2.64
Pr_2CoIn_8	4.615	12.193	259.689	2.64
Nd_2CoIn_8	4.608	12.172	258.456	2.64
Sm_2CoIn_8	4.583	12.101	254.168	2.64
Gd_2CoIn_8	4.57	12.021	250.948	2.63
Tb_2CoIn_8	4.568	12.008	250.566	2.63
Dy_2CoIn_8	4.561	11.99	249.425	2.63
Ho_2CoIn_8	4.55	11.98	246.927	2.63
Y_2CoIn_8	4.574	12.01	251.267	2.63

Table 2. Crystallographic parameters for the Dy_2CoIn_8 compound. For compounds with other rare earths only the temperature factor (U_{eq}) will change.

Atom	Site symmetry	x	y	z	U_{eq} (Å^2)	Occupancy
Dy	2g	0.00	0.00	0.306	0.989	2
Co	1a	0.00	0.00	0.000	0.875	1
In	2e	0.00	0.50	0.500	0.058	2
In	2h	0.50	0.50	0.308	0.023	2
In	4i	0.00	0.50	0.118	0.107	4

3. Results and discussions

The R_2CoIn_8 series of compounds forms in a Ho_2CoGa_8-type tetragonal structure with space group $P4/mmm$. In order to confirm the phase homogeneity of the compound with proper lattice and crystallographic parameters, a Rietveld analysis of the x-ray patterns of all the compounds was done using the FullProf program. The lattice parameters thus obtained are presented in table 1 and the refined plot for Dy_2CoIn_8 is shown in figure 1. The refined crystallographic parameters for each of the constituent atoms (at various crystallographic sites) in Dy_2CoIn_8 are presented in table 2. The site symmetry (table 2) will remain the same for all the compounds in the series. The crystal structure generated by the FullProf program after refinement of the x-ray pattern is shown in figure 2. The black lines connecting the Co atoms represent a unit cell. The central portion of the R_2CoIn_8 unit cell (figure 2) between the rare

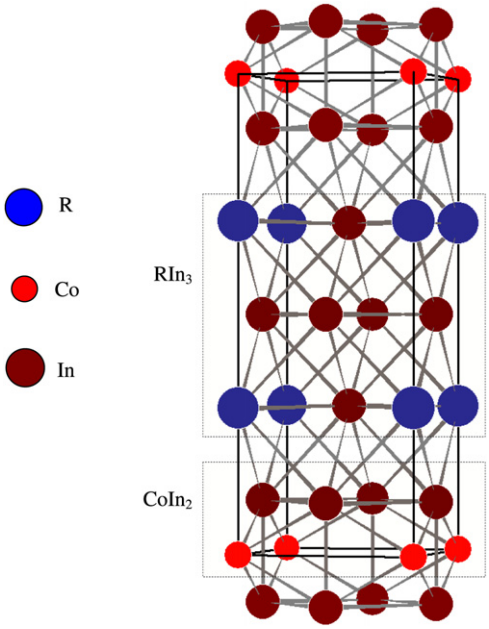

Figure 2. Tetragonal unit cell of R_2CoIn_8 compound. The dark lines connecting the Co atoms represent a unit cell.

earth planes (along the c axis) and including them represents a unit cell of the RIn_3 phase. The lattice parameters (a and b) of R_2CoIn_8 compounds are also approximately equal to that of their corresponding RIn_3 compounds (cubic phase) [11]. The remaining Co–In structure below and above the RIn_3 unit cell forms a $CoIn_2$ layer. Hence the R_2CoIn_8 unit cell can be considered as a RIn_3 unit cell sandwiched between the two $CoIn_2$ layers along the c axis [12]. The unit cell volumes of the R_2CoIn_8 compounds are plotted against their corresponding rare earths in figure 3(a). The volume decreases as we move towards heavier rare earths, and this is attributed to the well-known lanthanide contraction. The decrease in the unit cell volume is nearly smooth, without any sharp anomaly, indicating a similar valence of the rare earth ion (R^{3+}) in all the compounds. The average ratio of lattice parameters (c/a) of the compounds is $\approx$3.644, indicating a huge anisotropy in the crystal structure. The high structural anisotropy of the compound affects the other physical behaviours of the compound.

The R_2CoIn_8 compounds exhibit the following properties. Y_2CoIn_8 is Pauli paramagnetic down to 2 K. Ce_2CoIn_8 shows a heavy fermion behaviour. Pr_2CoIn_8 shows a crystal field effect at low temperature. Compounds with other magnetic rare earths (Nd, Sm, Gd, Tb, Dy and Ho) show antiferromagnetic ordering at low temperatures (table 3). The transition temperature of R_2CoIn_8 compounds decreases compared to that of RIn_3 (the basic building block for the compound) compounds except for Nd_2CoIn_8. In the case of Nd_2CoIn_8, the transition temperature ($\approx$10 K) is increased compared to that of $NdIn_3$ (7 K). According to the de Gennes scaling, the T_N of the isostructural members of the rare earth series is proportional to $(g_J - 1)^2 J(J + 1)$, where g_J is the Landé factor and J is the total angular momentum. The Néel temperature (T_N) of the R_2CoIn_8 series of compounds is plotted with their corresponding expected values from the de Gennes scaling in figure 3(b). The Néel temperatures of Nd_2CoIn_8 and Tb_2CoIn_8 vary appreciably from their expected values. This may be attributed to the crystal field effects. A crystal field is found to enhance the magnetic transition temperature in some cases [13]. Because of the structural anisotropy of the compounds the crystal field plays a crucial role in determining the properties of the compounds.

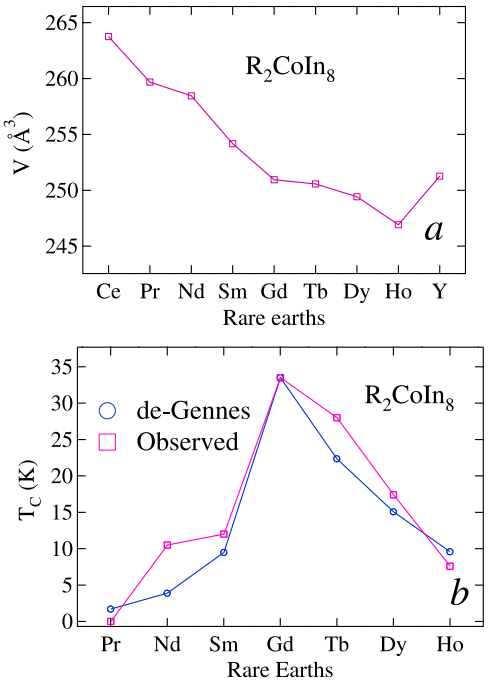

Figure 3. (*a*) Variation of unit cell volume with rare earths. (*b*) Néel temperature of the R_2CoIn_8 compounds compared with that expected from de Gennes scaling. The lines joining the data points are a guide to the eye.

Table 3. Neél temperatures for RIn_3 and the R_2CoIn_8 series of compounds. Paramagnetic Curie temperature (θ_P) and effective magnetic moment (μ_{eff}) for R_2CoIn_8 compounds. (Note: HF = heavy fermion; P–P = Pauli paramagnet; P = paramagnet.)

	RIn_3	R_2CoIn_8		
R	T_N (K)	T_N (K)	θ_P (K)	$\mu_{eff}(\mu_B)$
Y	P–P	P–P	—	—
Ce	HF	P	−25	2.2
Pr	P	P	−3	2.6
Nd	7	10	−12	3.6
Sm	16	12	−7.5	0.7
Gd	45	33.5	−39.5	7.9
Tb	36	30	−19	9.7
Dy	23	17.4	−11	10.6
Ho	11	7.6	−12	10.4

3.1. Y_2CoIn_8

In order to verify whether or not the magnetism arises from the magnetic transition element Co, the magnetic susceptibility of the non-magnetic rare earth compound Y_2CoIn_8 was measured first; this is shown in figure 4(*a*). The curve is nearly temperature independent, representing a Pauli paramagnetic behaviour. There is a slight upturn at low temperatures, which may be due to a small paramagnetic impurity in the sample. In order to ascertain the effect of such an impurity phase, the susceptibility was fitted to a modified Curie–Weiss law given by

$$\chi = \chi_0 + \frac{C_{CW}}{T - \theta_P}. \tag{1}$$

The fit gives $\chi_0 = 5.8 \times 10^{-3}$ emu/mol and an effective moment of 0.05 μ_B (a better fit at low temperature would give a moment value even less then this). Such a small value of effective

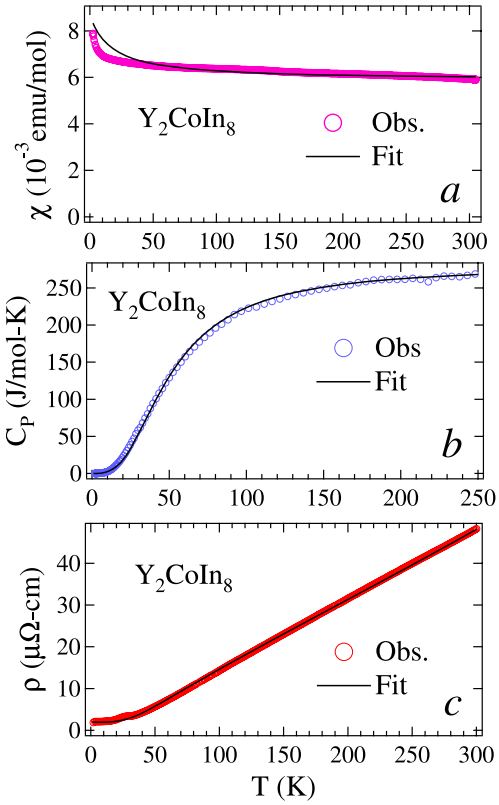

Figure 4. (*a*) Susceptibility of Y_2CoIn_8 fitted to modified Curie–Weiss law. (*b*) Heat capacity curve for the same with a fit. (*c*) Resistivity curve for the same fitted to a Bloch–Grüneisen relation.

moment and a huge value of χ_0 indicate that the upturn in the susceptibility at low temperatures is due to some minor impurity in the sample. Such a behaviour is expected for a compound with a non-magnetic ground state. This shows that Co is non-magnetic in this series of compounds. The resistivity behaviour of Y_2CoIn_8 (figure 4(*c*)) is as expected for a non-magnetic compound (pure phonon contribution). A small hump appears at approximately 30 K whose origin is not known. The behaviour of such a non-magnetic compound can be described by the modified Bloch–Grüneisen relation

$$\rho(T) = \rho_0 + 4R\Theta_D\left(\frac{T}{\Theta_D}\right)^5 \int_0^{\Theta_D/T} \frac{x^5 dx}{(e^x - 1)(1 - e^x)} - KT^3$$
$$x = \frac{\Theta_D}{T} \tag{2}$$

where ρ_0 is the temperature-independent residual resistivity, the second term (which goes as T^5) accounts for the electron–phonon scattering process and the third term (giving a T^3 contribution) arises due to the Mott s–d interband scattering. The notation Θ_D represents the Debye temperature and the coefficients R and K stand for electron–phonon and s–d interactions, respectively. The fit to the resistivity curve yields the following values of the parameters: $\Theta_D = 211$ K, $R = 0.156\ \mu\Omega$ cm K^{-1}, $K = 0.05 \times 10^{-7}\ \mu\Omega$ cm K^{-3} and $\rho_0 = 1.5\ \mu\Omega$ cm. The coefficient for electron–phonon interaction is higher compared to that of copper ($R = 0.03\ \mu\Omega$). The temperature-independent resistivity arises at very low temperatures due to the scattering of the conduction electrons by the impurities and the defects in the sample. At low temperatures the phonon contribution becomes vanishingly small and hence contributions from impurities/imperfections dominate. The residual resistivity ratio

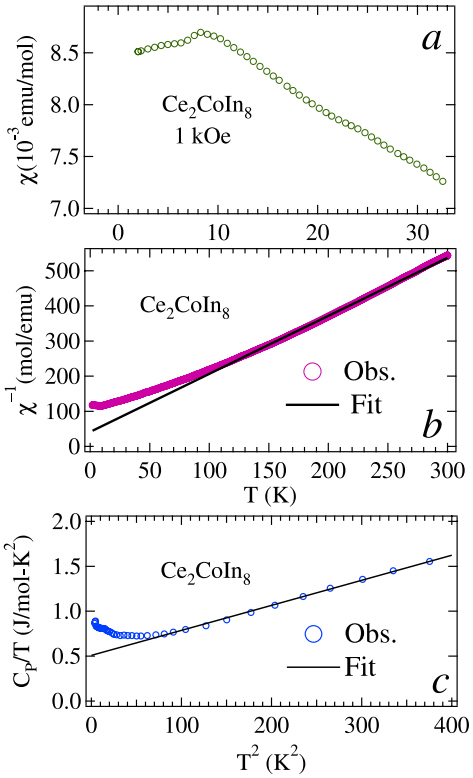

Figure 5. (*a*) Low-temperature susceptibility of Ce_2CoIn_8. (*b*) Inverse susceptibility fitted to the Curie–Weiss law. (*c*) Low-temperature part of the C_P/T versus T^2 curve for the same fitted to a straight line.

($\rho(300\ \mathrm{K})/\rho(2\ \mathrm{K}) \approx 33$) and $\rho_0 = 1.5\ \mu\Omega$ suggest a good sample quality in the case of polycrystalline samples. The value of residual resistivity ρ_0 goes below 1 $\mu\Omega$ for single crystals. The heat capacity behaviour of the compound also reflects the non-magnetic behaviour of the compound (figure 4(*b*)). It could be fitted to the equation

$$C_{\mathrm{Tot}} = C_{\mathrm{elec}} + C_{\mathrm{Ph}} = \gamma T + \beta T^3. \tag{3}$$

The first term represent the electronic contribution, and the second the phononic contribution. The phononic contribution in terms of Debye integral can be written as

$$C_{\mathrm{Ph}} = 9NR\left(\frac{T}{\Theta_{\mathrm{D}}}\right)^3 \int_0^{\Theta_{\mathrm{D}}/T} \frac{x^4 \mathrm{e}^x \mathrm{d}x}{(\mathrm{e}^x - 1)^2} \qquad x = \frac{\Theta_{\mathrm{D}}}{T} \tag{4}$$

where N is the number of atoms in the formula unit and Θ_{D} is the Debye temperature. The best fit was obtained by considering the following values: $N = 11$, $\Theta_{\mathrm{D}} = 211$ K and $\gamma = 13$ mJ/mol-K^2. The value of γ was estimated from the straight line intercept of the C_P/T versus T^2 curve (not shown). This shows that the specific heat curve of Y_2CoIn_8 can well describe the phonon contribution of the R_2CoIn_8 compounds. (The data have to be renormalized with respect to the molecular mass of the corresponding rare earth compound, as described elsewhere [22].)

3.2. *Ce_2CoIn_8*

The low-temperature magnetic susceptibility, $\chi(T)$, of Ce_2CoIn_8 is shown in figure 5(*a*). The susceptibility increases with decrease in temperature (as expected for free spin paramagnetism) followed by a small hump at ≈8 K, and becomes nearly temperature independent at low

temperatures. The exact reason for the origin of the hump is not known. A similar hump in Ce_2CoIn_8 at approximately the same temperature was also reported by Chen *et al* [9] in their single-crystal measurement. Such a hump is also found in $CeRhIn_5$ [3] and is attributed to be arising from orbitally degenerate Kondo impurities [14]. Considering this, we attribute the hump at ≈8 K to be arising from the ground state of Ce ions (considered as Kondo impurities). The nearly temperature-independent susceptibility at low temperatures is the characteristic of heavy fermion compounds. The inverse molar susceptibility, $\chi^{-1}(T)$, plotted in figure 5(*b*), follows a linear temperature dependence above 100 K. The Curie–Weiss fit gives an effective moment of 2.2 μ_B and a Curie temperature of −25 K. The value of the effective moment obtained is less than the value expected for a free Ce^{3+} ion (2.54 μ_B). The deviation of the $\chi^{-1}(T)$ curve from a straight line below 100 K can be attributed to crystal field effects and/or Kondo-type interactions. The large negative paramagnetic Curie temperature suggests the presence of strong antiferromagnetic and/or Kondo-type interactions. The Kondo-type behaviour is evident in the resistivity behaviour of the compound discussed below, and hence we attribute the observed behaviour to the Kondo-type interaction present in the compound.

Reports on the heat capacity results of Ce_2CoIn_8 (single crystal) [8] shows a heavy fermion behaviour of the compound with $\gamma = 500$ mJ/mol-K^2-Ce. Figure 5(*c*) shows the C_P/T versus T^2 curve for Ce_2CoIn_8. The curve decreases linearly with temperature up to ≈80 K^2 and then deviates, showing an upward turn at low temperature. The obtained value of $\gamma = 460$ mJ/mol-K^2-Ce is low compared to the reported one [8]. The upward turn at low temperature may be due to the presence of a Schottky anomaly or spin fluctuation [15]. A heavy fermion means an increase in the effective mass of the conduction electrons. The effective mass of the electron is given by

$$m^* = \frac{\hbar^2 k_F^2 \gamma}{\pi^2 (Z/\Omega) k_B^2} \tag{5}$$

where k_F is the Fermi wavevector given by $k_F = (3\pi^2 Z/\Omega)^{1/3}$, and Z is the number of conduction electrons per unit cell; we assume that Ce contributes three electrons per atom ($Z = 6$). Ω is the unit cell volume (263.75 Å^3). Other symbols have their usual meaning. Substituting the value in the above equation ($\gamma = 920$ mJ/mol-K^2) we get $m^* \approx 55 m_e$, where m_e is the mass of a free electron. In the case of heavy fermion compounds the Wilson ratio (ratio of the susceptibility to that of the electronic specific heat) is calculated, given by

$$\frac{\chi_0}{\gamma} = \frac{3\mu_B^2}{\pi^2 k_B^2} \tag{6}$$

where χ_0 is the susceptibility at 0 K and the other parameters have their usual meanings. The ratio has an ideal value of 1.372×10^{-9}, whereas our experimental value comes out to be 1.8×10^{-9}. The reason for the higher value of the ratio is not known.

The magnetic contribution to the specific heat of the compound was isolated by subtracting the specific heat of the non-magnetic counterpart Y_2CoIn_8 after renormalizing it by atomic mass. The magnetic contribution to the entropy was then calculated using the relation

$$S(T)_{mag} = \int_0^T \frac{C(T)_{mag}}{T} dT. \tag{7}$$

The calculated value of entropy comes out to be 14.2 J/mol-K-Ce, which is less than the theoretically expected value $R \times \ln(2J + 1) = 14.8$ J/mol-K, where $J = 5/2$ for Ce^{3+} ion and $R = 8.314$ J/mol-K is the gas constant. The exact reason for the low value is not known, but a possibility can be attributed to the Kondo behaviour or crystal field effects.

Figure 6 shows the resistivity of Ce_2CoIn_8 as a function of temperature. The curve is typical for materials showing heavy fermion/Kondo behaviour. When the temperature is

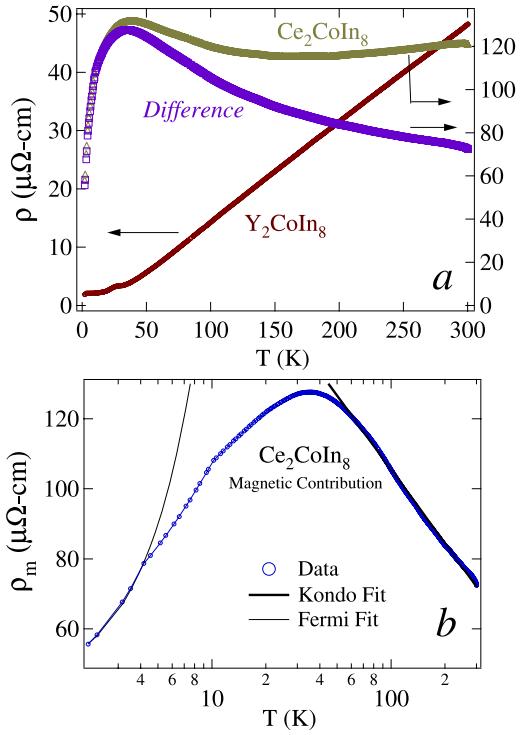

Figure 6. (*a*) Resistivity of Ce_2CoIn_8 and Y_2CoIn_8 along with their difference [$\rho(Ce_2CoIn_8)$–$\rho(Y_2CoIn_8)$] indicated by *difference*; the arrows represent their respective scales. (*b*) Magnetic contribution to the resistivity fitted to the Kondo equation at high temperature; the low temperature part was fitted for the verification of the Fermi liquid behaviour.

decreased from 300 K, initially the resistivity decreases with decrease in temperature. This shows a dominant phononic behaviour at high temperature. At approximately 160 K the resistivity shows minima and then increases with temperature. The increase in resistivity is due to the dominating Kondo lattice behaviour; it is the scattering of the conduction electrons by the Kondo impurity. In the case of Ce_2CoIn_8, the 4f electrons of Ce^{3+} ions immersed in the Fermi sea of conduction electrons give rise to Kondo behaviour. The resistivity then shows a peak at ≈35 K and then decreases rapidly with temperature. This behaviour is generally attributed to a crossover from strongly incoherent scattering of conduction electron at high temperature to the development of strongly correlated block states at low temperature. Below ≈10 K the resistivity is linear in temperature; such a functional dependence is commonly found in the case of magnetically mediated superconductors [16]. The magnetic contribution to the total resistivity of the compound was separated by subtracting the phonon contribution. Now, we assume that the phonon contribution to the resistivity of Ce_2CoIn_8 is well described by its non-magnetic counterpart Y_2CoIn_8. The total resistivity is written as

$$\rho_{\mathrm{Tot}}(Ce_2CoIn_8) = \rho_0(Ce_2CoIn_8) + \rho_{\mathrm{Ph}}(Y_2CoIn_8) + \rho_{\mathrm{mag}}(Ce_2CoIn_8) \tag{8}$$

where

$$\rho_{\mathrm{Ph}}(Y_2CoIn_8) = \rho_{\mathrm{Tot}}(Y_2CoIn_8) - \rho_0(Y_2CoIn_8).$$

The magnetic contribution ($\rho_0 + \rho_{\mathrm{mag}}$) for Ce_2CoIn_8 separated by this procedure is plotted in figure 6(*a*) on a linear temperature scale and in figure 6(*b*) on a log scale. Since the resistivity

of Ce_2CoIn_8 does not saturate down to 2 K, the separated magnetic part also consists of ρ_0. The following analysis will include the residual resistivity ρ_0. The high-temperature part of the resistivity ($\approx$ above 50 K) shows a dominant Kondo behaviour, and it could be fitted to the Kondo formula given by

$$\rho_{\text{mag}} = \rho_0^{\text{SDR}} - c_{\text{K}} \ln(T) \tag{9}$$

where $\rho_0^{\text{SDR}} = \rho_0 + \rho_{\text{SDR}}$, c_{K} is the Kondo coefficient and ρ_{SDR} is the spin disorder resistivity. Both ρ_{SDR} and ρ_0 are independent of temperature. The best fit to the resistivity curve (figure 6(*b*)) of the above equation was obtained with $\rho_0^{\text{SDR}} = 246\ \mu\Omega$ cm and $c_{\text{K}} = 70\ \mu\Omega$ cm. The Kondo coefficient has a value that is moderately high compared to those of other heavy fermion compounds ($CeIn_3$, Ce_2Pt_2In, etc: 200–300 $\mu\Omega$). According to Kondo's theory [17], the Kondo coefficient is proportional to the density of states at the Fermi level. This indicates a moderately high density of states at the Fermi level compared to other heavy fermion compounds. The low-temperature part of the resistivity curve is fitted to the equation

$$\rho(T) = \rho_0 + AT^x \tag{10}$$

with $\rho_0 = 43.8\ \mu\Omega$ cm, $A = 4.2\ \mu\Omega$ cm K^{-2} and $x = 1.5$. The deviation of the resistivity curve from pure quadratic behaviour ($x = 2$) indicates the non-Fermi liquid behaviour of the compound. Similar results were also obtained for $CeIrIn_5$, $CeRhIn_5$, Ce_2CoIn_8 and Ce_2IrIn_8 [3, 6, 9]. Such a behaviour in a heavy fermion compound can be possibly attributed to spin fluctuation. The absence of magnetic ordering of Ce ions also supports the possible presence of spin fluctuation [18].

3.3. Pr_2CoIn_8

The susceptibility of Pr_2CoIn_8 (figure 7(*a*)) increases with decrease in temperature and becomes nearly temperature independent at low temperature (below $\approx$20 K). The behaviour is similar to that of a ferromagnetic compound. To check this, a magnetic isotherm was measured at 2 K and up to 70 kOe (figure 7(*c*)). The linear behaviour of the magnetic isotherm rules out the ferromagnetic ordering of the compound, reflecting only the possibility of paramagnetic behaviour. Such a behaviour is also found under the dominating crystal field effects [11]. The crystal field splits the $2J + 1$-fold degenerate ground state to several sublevels. In the case of a rare earth ion possessing an even number of 4f electrons, a non-magnetic ground state is expected, a non-magnetic singlet [11] or rarely a non-magnetic doublet [20]. The non-magnetic ground state would remain stable down to very low temperature if the exchange interactions do not exceed a certain critical value [21]. In such cases, temperature-independent Van Vleck susceptibility is expected at low temperatures. In the case of Pr_2CoIn_8, only Pr is magnetic and the Pr^{3+} ion has two 4f electrons, making it a suitable candidate for such a behaviour. Therefore, in order to demonstrate the presence of the crystal field effects, we have considered the Hamiltonian with two leading terms given by

$$H_{\text{CEF}} = B_2^0 O_2^0 + B_2^2 O_2^2$$

where O_n^m are the Steven's operators in terms of the angular momentum operators and B_n^m are the constants which measure the strength of the crystal field. The diagonalization of the above Hamiltonian together with other detailed calculation was done using the computer simulation of the standard procedure described elsewhere [19]. The $\chi^{-1}(T)$ curve for Pr_2CoIn_8 was fitted as shown in figure 7(*b*). The eigenfunctions and the eigenenergy values thus obtained under zero-field conditions are given in table 3. The dominant crystal field parameters B_2^0 and B_2^2 have the values 1.55 and 1.89 K respectively. The ground state is a non-magnetic doublet, which is rarely found. A few reported cases are $TmIn_3$ and $TmAl_3$ [20, 23]. Figure 8(*a*) shows the

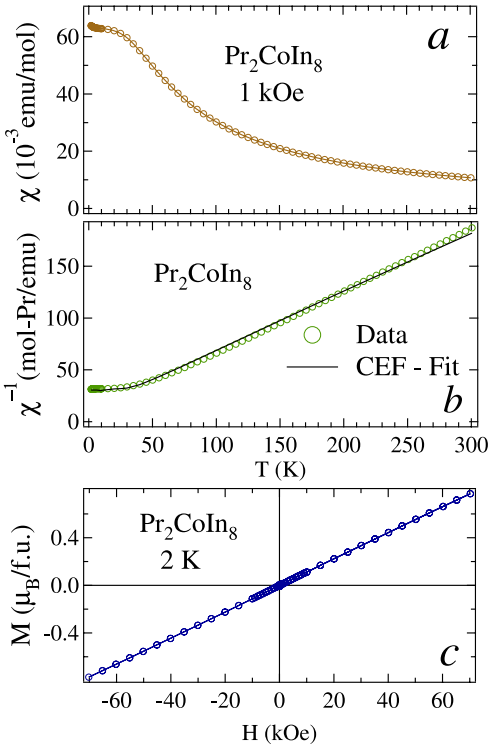

Figure 7. (*a*) Susceptibility of Pr_2CoIn_8 measured at 1 kOe. (*b*) Inverse susceptibility for the same with crystal field fit. (*c*) Magnetic isotherm for the same at 2 K. In (*a*) and (*c*) the lines joining the data points are guides to the eye.

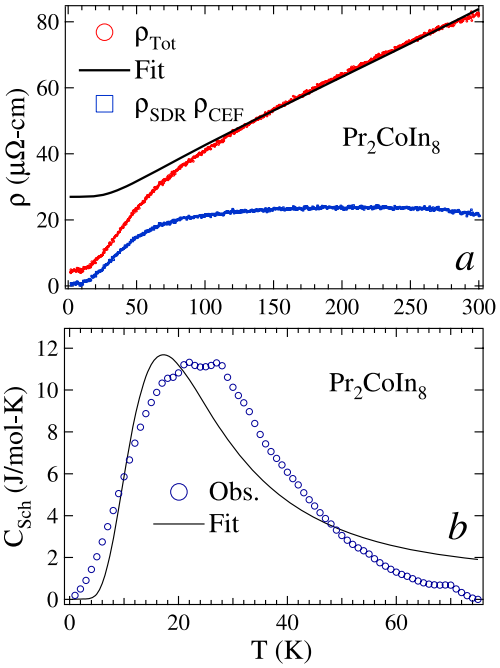

Figure 8. (*a*) Resistivity of Pr_2CoIn_8 fitted to the Bloch–Grüneisen relation with spin disorder resistivity (ρ_{SDR}) added to it. The other curve is the pure spin disorder resistivity affected by crystal field effect at low temperature ($\rho_{SDR}\,\rho_{CEF}$). (*b*) Schottky contribution to the specific heat for the same fitted to the equation in the text.

total resistivity curve for Pr_2CoIn_8 from 2 to 300 K. The curve is fitted to the Bloch–Grüneisen relation (equation (2)). Since there is no magnetic ordering down to 2 K, the deviation of

Table 4. Energy levels, degeneracy and wavefunctions for the crystal field split $J = 4$ state in the absence of magnetic field for Pr_2CoIn_8

Energy (K)	Degeneracy	Wavefunction
0	2	$0.0443\,\|\pm4\rangle - 0.4096\,\|\pm2\rangle + 0.8127\,\|0\rangle$
		$0.1719\,\|\pm3\rangle + 0.6859\,\|\pm1\rangle$
33	1	$-0.3463\,\|\pm3\rangle + 0.6164\,\|\pm1\rangle$
35	1	$\pm0.1212\,\|\pm4\rangle \mp 0.6966\,\|\pm2\rangle$
53	1	$-0.1408\,\|\pm4\rangle + 0.5591\,\|\pm2\rangle + 0.5789\,\|0\rangle$
64	1	$\pm0.6858\,\|\pm3\rangle \pm 0.1719\,\|\pm1\rangle$
68	1	$0.6164\,\|\pm3\rangle + 0.3463\,\|\pm1\rangle$
94	2	$\mp0.6966\,\|\pm4\rangle \mp 0.1212\,\|\pm2\rangle$
		$0.6915\,\|\pm4\rangle - 0.1401\,\|\pm2\rangle + 0.0658\,\|0\rangle$

the resistivity from the expected path (below ≈110 K) can be attributed to the crystal field effect. The fit to the experimental curves above 110 K gives the values $\Theta_D = 211$ K, $R = 0.19\ \mu\Omega$ cm K^{-1}, $K = 0.2 \times 10^7 \mu\Omega$ cm K^{-3} and $\rho_0^{SDR} = 27\ \mu\Omega$ cm, where $\rho_0^{SDR} = \rho^0 + \rho^{SDR}$; the spin disorder resistivity (ρ^{SDR}) could not be excluded since the compound is in the paramagnetic state up to the lowest temperature. We compare the values with those obtained for Y_2CoIn_8 ($\Theta_D = 211$ K, $R = 0.156\ \mu\Omega$ cm K^{-1}, $K = 0.05 \times 10^{-7} \mu\Omega$ cm K^{-3} and $\rho_0 = 1.5\ \mu\Omega$ cm). The Debye temperature remains the same, but the electron–phonon coefficient R has increased in the case of Pr_2CoIn_8 compared to the latter one. This implies that the electron–phonon interaction has increased in the case of Pr_2CoIn_8. This result is also supported by the value of the electronic specific heat coefficient γ which has a value that is larger in the case of Pr_2CoIn_8 (21.3 mJ/mol-K^2) than Y_2CoIn_8 (13 mJ/mol-K^2). Subtracting the phonon contribution from the total resistivity gives a constant spin disorder resistivity (≈23 $\mu\Omega$ at high temperature >100 K) with a crystal field effect at low temperature (figure 8(*a*)). The crystal field effect on spin disorder resistivity (figure 8(*a*)) could not be fitted with the energy levels obtained from the magnetization measurement. The electronic contribution from the heat capacity curve (not shown) of Pr_2CoIn_8 comes out to be 21.3 J/mol-K^2. Taking this into account and renormalizing the Y_2CoIn_8 heat capacity data, the magnetic contribution to the heat capacity of Pr_2CoIn_8 was isolated (figure 8(*b*)). The magnetic entropy calculated using equation (7) is 17.2 mJ/mol-K^2-Pr. The value is less than that expected for a Pr^{3+} ion (18.2 mJ/mol-K^2). The reason is due to the crystal field effects. The crystal field energy levels calculated from the magnetization measurement in table 4 were used to calculate the Schottky contribution to the heat capacity using the equation

$$C_{Sch}(T) = R\left[\frac{\sum_i g_i e^{-E_i/T} \sum_i g_i E_i^2 e^{-E_i/T} - \left[\sum_i g_i E_i e^{-E_i/T}\right]^2}{T^2\left[\sum_i g_i e^{-E_i/T}\right]^2}\right]$$

where R is a gas constant, E_i is the energy in units of temperature and g_i is the degeneracy of the energy level. The curve obtained using the above equation is plotted with the experimentally determined Schottky anomaly in figure 8(*b*). The agreement is not good; this may be due to the various approximations taken into account in the magnetization fit.

3.4. Gd_2CoIn_8

The low-temperature susceptibility of Gd_2CoIn_8 is shown in figure 9(*a*) for applied fields of 0.2 and 50 kOe. The susceptibility at 0.2 kOe shows an antiferromagnetic transition at ≈33.5 K and then shows an upward turn at ≈5 K. The susceptibility at 50 kOe also shows an upward turn

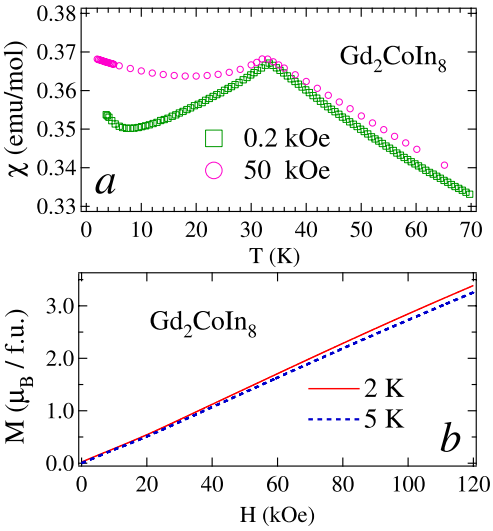

Figure 9. (*a*) Susceptibility of Gd_2CoIn_8 measured at 0.2 and 50 kOe. (*b*) Magnetic isotherm for the same at 2 and 5 K.

at low temperatures. The upward turn at low temperatures may be due to some paramagnetic impurity in the sample (undetected in the x-ray diffraction pattern) or due to a spin reorientation with a ferromagnetic component arising at low temperatures. However, the magnetic isotherm at 2 K (figure 9(*b*)) shows a straight line behaviour, which excludes the presence of any ferromagnetic component in the compound at that temperature. The inverse susceptibility fit to the Curie–Weiss law gives an effective moment of 7.9 μ_B and a paramagnetic Curie temperature of −39.5 K (table 3). The large negative value of the paramagnetic Curie temperature also indicates a strong antiferromagnetic interaction among the Gd moments. The heat capacity curve of Gd_2CoIn_8 (figure 10(*a*)) shows an anomaly at the Néel temperature. The magnetic entropy obtained is 17.1 J/mol-K-Gd, (figure 10(*a*) inset) which is close to the expected value of 17.28 J/mol-K-Gd. The resistivity curve also drops form the normal metallic behaviour at T_N (figure 10(*b*)) because of the vanishing spin disorder resistivity. In the ordered state the resistivity is proportional to T^2; such a behaviour is expected for an isotropic ferromagnet [24] or Fermi liquid behaviour. A T^3 behaviour is expected for isotropic antiferromagnets [24]. The exact reason for the T^2 behaviour even though the compound shows antiferromagnetic ordering is not clear. The magnetoresistance (MR) of the compound at 2 K and 9 T in per cent is shown in figure 10(*c*). It was calculated using the relation

$$\mathrm{MR}\% = \frac{\rho(H) - \rho(0)}{\rho(0)} \times 100. \tag{11}$$

It shows a monotonic increase of the positive magnetoresistance with an ≈200% rise at 9 T, as expected for an antiferromagnet.

3.5. Dy_2CoIn_8

The low-temperature part of the susceptibility for Dy_2CoIn_8 is shown in figure 11(*a*). The susceptibility at 1 kOe reveals an antiferromagnetic transition at 17.4 K and another magnetic transition at 5 K. The transition at 5 K may be due to the reorientation of the spin with temperature. The susceptibility in the paramagnetic state was fitted to the modified Curie–Weiss law (equation (1)) with $\chi_0 = 0.028$ emu/mol, $\mu_{\mathrm{eff}} = 10.6\ \mu_B$ and a paramagnetic Curie temperature of −11 K. The negative value of paramagnetic Curie temperature suggests

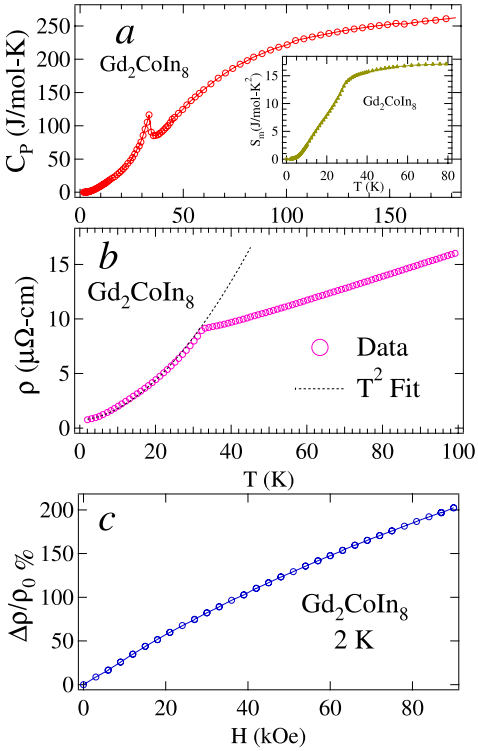

Figure 10. (*a*) Heat capacity of Gd_2CoIn_8 with an inset showing its magnetic entropy. (*b*) Low-temperature resistivity of Gd_2CoIn_8 with a T^2 proportionality fit. (*c*) Magnetoresistance for the same at 2 K and up to 90 kOe. In (*a*) and (*c*) the lines joining the data points are guides to the eye.

an antiferromagnetic interaction in the paramagnetic state. Applying a field of 50 kOe, the antiferromagnetic peak at 17 K gets broadened and shifts towards low temperature, and the magnetic transition at 5 K disappears and the susceptibility increases at low temperature. At 90 kOe the susceptibility becomes similar to that of a ferromagnetic compound, saturating at low temperatures (below 5 K). In order to further investigate the behaviour, the magnetic isotherm was measured at 2, 8 and 25 K (figure 11(*b*)). At 2 K the magnetic isotherm follows a straight line up to ≈37 kOe, confirming an antiferromagnetic behaviour of the compound at 2 K. The curve then undergoes two metamagnetic transitions at 38 and 82 kOe; at 8 K the sharpness of the metamagnetic transition decreases and at 25 K the straight line indicates the paramagnetic behaviour of the compound. The metamagnetic transition at 38 kOe is in agreement with the disappearance of the 5 K peak at 50 kOe in the magnetization versus temperature curve. The magnetic moment at 120 kOe and 2 K is 7.2 μB/f.u. Dy; such a high value of moment is possible only in the case of ferromagnetic behaviour of the compound. The heat capacity curve of the compound at zero fields also shows two anomalies at 5 and 17 K, similar to that in the magnetization measurements. In the field of 50 kOe the anomaly at 5 K disappears and that at 17 K shifts towards low temperature and gets broadened. At 90 kOe the anomaly vanishes and the curve shows only two broad humps. The resistivity of Dy_2CoIn_8 shows a metallic behaviour down to 17 K, after which an abrupt decrease in the resistivity is consistent with the loss of the spin disorder resistivity. The resistivity behaviour of the compound in the antiferromagnetically ordered state is given by [24]

$$\rho = \rho_0^S + b\Delta^2\sqrt{\frac{k_B T}{\Delta}}e^{-\Delta/k_B T}\left[1 + \frac{2}{3}\left(\frac{k_B T}{\Delta}\right) + \frac{2}{15}\left(\frac{k_B T}{\Delta}\right)^2\right] \tag{12}$$

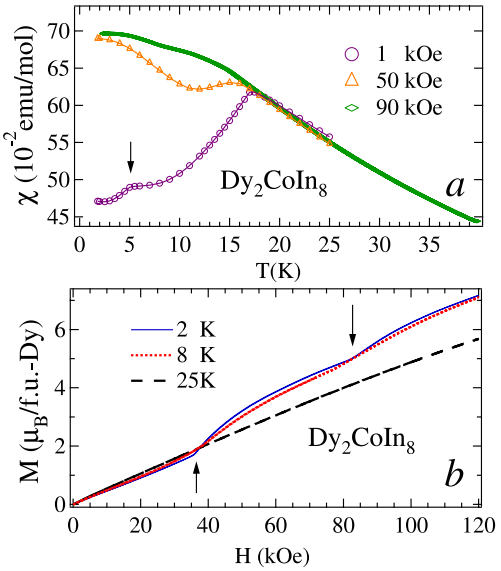

Figure 11. (*a*) Susceptibility of Dy_2CoIn_8 measured at 1, 50, and 90 kOe. The lines joining the data points are guides to the eye. (*b*) Magnetic isotherm for the same at 2, 8 and 25 K. The arrows indicate the metamagnetic transitions.

where b is a constant and Δ represents the anisotropy energy gap, and ρ_0^S represents the sum of the residual resistivity and the spin disorder resistivity in the ordered state, if present. Here we assume that the lowest value of the observed resistivity at 2 K is equal to ρ_0. The resistivity data in the ordered state could be fitted to the two different curves generated by the above equation for two different values of ρ_0^S and the same values of Δ and b. The curve fitted to the data above $\approx$5 K gives $\rho_0^S = 2.3\ \mu\Omega$ cm and that below $\approx$5 K gives $\rho_0^S = 1.4\ \mu\Omega$ cm (ρ_0) with $\Delta = 4$ K and $b = 0.043\ \mu\Omega$ cm K^{-1}. The lower value of ρ_0^S below 5 K suggests that the spins are in more ordered state compared to the state above 5 K. Now considering the anomaly in the specific heat and magnetization measurements at approximately the same temperature, we suggest that the anomaly at 5 K is due to the reorientation of the spins. The magnetoresistance of the compound at 2 K (figure 12(*c*)) increases initially with increase in temperature as expected for an antiferromagnetic compound. After $\approx$83 kOe (approximately the field corresponding to the second metamagnetic transition) it starts decreasing with increasing field. The decrease in the magnetoresistance with field is attributed to the ferromagnetic nature of the compound. Hence, considering the magnetization results along with the magnetoresistance behaviour, we can say that the second metamagnetic transition transfers the compound to the ferromagnetic state. The highest change in magnetoresistance at 2 K is 250% at $\approx$82 kOe. Such a high value may be due to the structural anisotropy.

3.6. Ho_2CoIn_8

The low-temperature susceptibility of Ho_2CoIn_8 in various fields is shown in figure 13(*a*). The low-field susceptibility (1 kOe) indicates the presence of an antiferromagnetic transition at $\approx$7.5 K. The susceptibility at 40 kOe show a huge broadening of the antiferromagnetic peak and it shifts towards low temperatures, consistent with an antiferromagnetic ordering. At 80 kOe the peak vanishes altogether and the susceptibility increases with temperature. The inverse

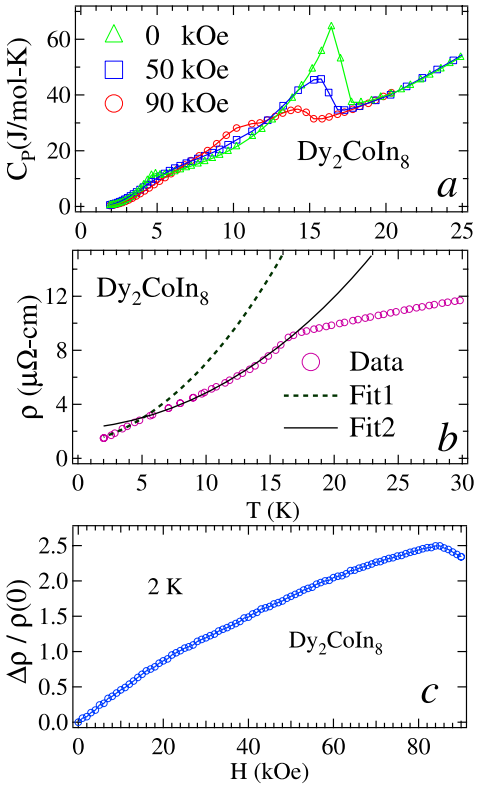

Figure 12. (*a*) Heat capacity of Dy_2CoIn_8 with an applied field of 0, 50, and 90 kOe. The lines joining the data points are guides to the eye. (*b*) Low-temperature resistivity of Dy_2CoIn_8 with a fit to the equation in the text. (*c*) Magnetoresistance for the same at 2 K and up to 90 kOe.

susceptibility in the paramagnetic region was fitted to the Curie–Weiss law with the parameters given in table 3. The linear behaviour of the magnetic isotherm at 2 K (fields below 20 kOe) (figure 13(*b*)) proves the antiferromagnetic behaviour of the compound. Increase in the field causes the compound to undergo two metamagnetic transitions, one at ≈25 kOe and the other at ≈55 kOe. Further increase in the field moves the curve towards saturation with a magnetization of ≈9.1 μ_B at 120 kOe. The magnetization value is near to the saturation value of the Ho^{3+} ion (10 μ_B). This suggests that the compound is nearly in the ferromagnetic state at 120 kOe.

The low-temperature heat capacity of the compound in various fields is shown in figure 14(*a*). When the magnetic field is zero, the heat capacity shows an anomaly at the antiferromagnetic transition temperature of the compound. Application of a field (50 kOe) broadens the peak and splits it into three different peaks. This may be due to the combined effect of magnetic and crystal field effects on the energy levels. At 90 kOe all the peaks vanish altogether, consistent with what is found in the magnetization behaviour.

The resistivity curve for Ho_2CoIn_8 is shown in figure 14(*b*). The resistivity shows its usual metallic behaviour down to the ordering temperature of ≈7.5 K and then drops rapidly below the ordering temperature. In the ordered state the resistivity was fitted to equation (12) with $\rho_0^S = 1.3\ \mu\Omega$ cm (ρ_0) with $\Delta = 2$ K and $b = 0.01\ \mu\Omega$ cm K^{-1} assuming the minimum resistivity at 2 K to be equal to $\rho_0(\rho_0^S = \rho_0)$. The magnetoresistance of the compound at 2 K is shown in figure 14(*c*) as a function of field. Initially the magnetoresistance

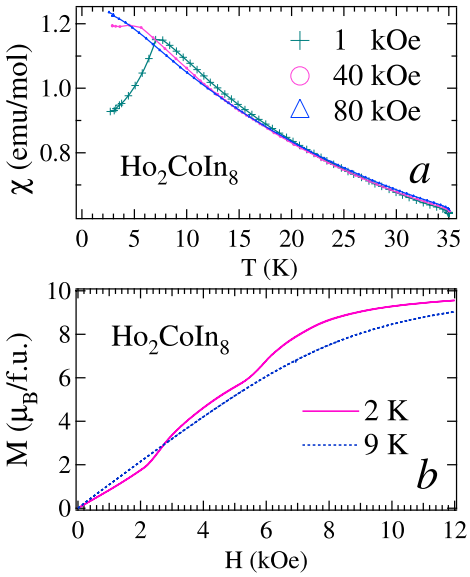

Figure 13. (*a*) Susceptibility of Ho_2CoIn_8 measured at 1, 40, and 80 kOe. The lines joining the data points are guides to the eye. (*b*) Magnetic isotherm for the same at 2 and 9 K.

increases with increase in the field, showing a behaviour typical for an antiferromagnet. At ≈22 kOe a signature of its deviation from the initial path is seen, which corresponds to the first metamagnetic transition in the magnetization isotherm. At ≈54 kOe the curve takes a downward turn and then decreases with field up to ≈80 kOe, after which it becomes nearly temperature independent. The decrease in the magnetoresistance again indicates the ferromagnetic state achieved by the compound after the second metamagnetic transition. After that the magnetoresistance becomes nearly independent of field (between 74 and 90 kOe). On decreasing the field, a hysteresis is found between 80 and 90 kOe; after that the curve follow the same path.

3.7. Sm_2CoIn_8

The low-temperature susceptibility of Sm_2CoIn_8 at 0.5, 1 and 50 kOe is shown in figure 15(*a*). The low-field susceptibility (0.5 kOe) shows an antiferromagnetic-type peak at ≈12 K and an upturn below 5 K. The susceptibility at 1 kOe also shows a similar behaviour, with an increased value. At 50 kOe the susceptibility shows a marginal increase (below 5 K) with broad minima. To further investigate the magnetic behaviour, the magnetization was measured as a function of applied field at 2 and 4 K (figure 16). The magnetic isotherm is very peculiar at 2 K. As the field is increased from zero, the magnetization remains almost zero initially and then increases linearly with field for $H > 4$ kOe (inset of figure 16). At $H \approx 26$ kOe, the magnetization shows a sharp increase, reminiscent of a metamagnetic transition. At still higher fields, the magnetization curve moves toward saturation. When the field is decreased, the curve shows a hysteretic behaviour similar to that of a ferromagnet. After that, within a complete hysteresis cycle the magnetization behaves like a ferromagnet, forgetting its original antiferromagnetic behaviour (a straight line in the M–H curve) at low fields in the virgin curve. At 4 K (upper inset of figure 16) the curve is almost a straight line with a small hysteresis clearly seen at high fields, and it is nearly zero at low fields (below 10 kOe). The magnetization values are

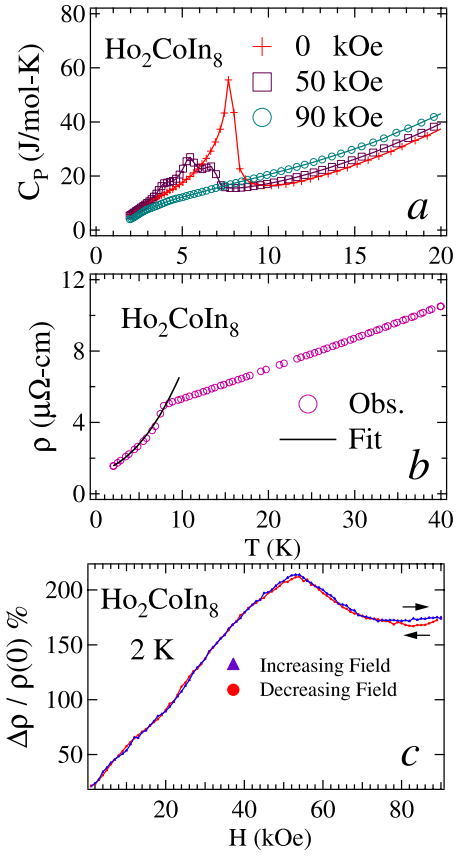

Figure 14. (*a*) Heat capacity of Ho_2CoIn_8 with an applied field of 0, 50, and 90 kOe. (*b*) Low-temperature resistivity of Ho_2CoIn_8 with a fit in ordered state to the equation in the text. (*c*) Magnetoresistance for the same at 2 K and up to 90 kOe. In (*a*) and (*c*) the lines joining the data points are guides to the eye.

less than half compared to that at 2 K. Before discussing these results in detail, let us look at other behaviour of the compound. The inverse susceptibility of the compound does not follow Curie–Weiss behaviour (figure 15(*b*)). The first excited state of the Sm^{3+} ion lies very near to the ground state ($\Delta E_{7/2-5/2} \approx 1400$ K). This results in thermally induced mixing of the excited states with the ground state. Hence the susceptibility in the paramagnetic state cannot be fitted to the Curie–Weiss law. The Curie–Weiss law modified to fit the susceptibility in such cases is given by [25]

$$\chi = \frac{N_A}{k_B}\left(\frac{\mu_{eff}^2}{3(T-\theta_P)} + \frac{\mu_B^2}{\delta}\right) \tag{13}$$

where N_A is the Avogadro number, k_B is the Boltzmann constant, μ_B is the Bohr magneton, μ_{eff} is the effective magnetic moment in units of μ_B, θ_P is the paramagnetic Curie temperature and $\delta = 7\Delta E/20$ in which ΔE is the difference between the ground state and the first excited state. For the Sm^{3+} ion, the first term in the above equation represents a Curie–Weiss contribution from the $J = 5/2$ ground state, while the second term is the temperature-independent Van Vleck correction arising from the accessible first excited $J = 7/2$ state. The solid line in figure 15(*b*) represents the fit to the data using equation (13) from 40 to 305 K. In the absence

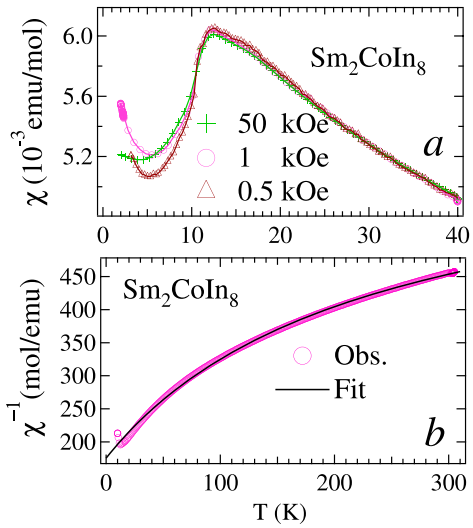

Figure 15. (*a*) Susceptibility of Sm_2CoIn_8 measured at 0.5, 1, and 50 kOe. The lines joining the data points are guides to the eye. (*b*) Inverse susceptibility for the same fitted to the modified Curie–Weiss law.

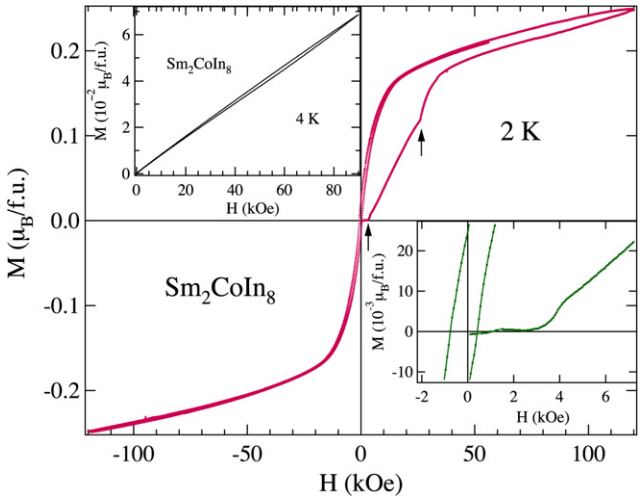

Figure 16. Magnetic isotherm of Sm_2CoIn_8 at 2 K with arrows indicating initial low-field behaviour and metamagnetic transition. The lower inset shows an expanded version of the same to depict the low-field behaviour. The upper inset shows the magnetic isotherm at 4 K.

of crystal field effects, the probable values of $\mu_{\rm eff}$ and δ are 0.845 $\mu_{\rm B}$ and 490 K, respectively. The values obtained from the susceptibility fit of Sm_2CoIn_8 are $\mu_{\rm eff} = 0.7\ \mu_{\rm B}$ and $\delta = 250$ K. The difference in the values of δ and $\mu_{\rm eff}$ can be attributed to the crystal field effects.

The resistivity behaviour of the compound is shown in figure 17(*b*). The resistivity follows a metallic behaviour almost down to the magnetic ordering temperature, followed by a drop due to the vanishing spin disorder resistivity. In the ordered state the resistivity data were fitted to equation (12), which gave the parameters as $\rho_0^S = 2.5\ \mu\Omega$ cm and $\Delta = 19$ K. The large value of the energy gap Δ indicates the huge anisotropy of the compound. The magnetoresistance

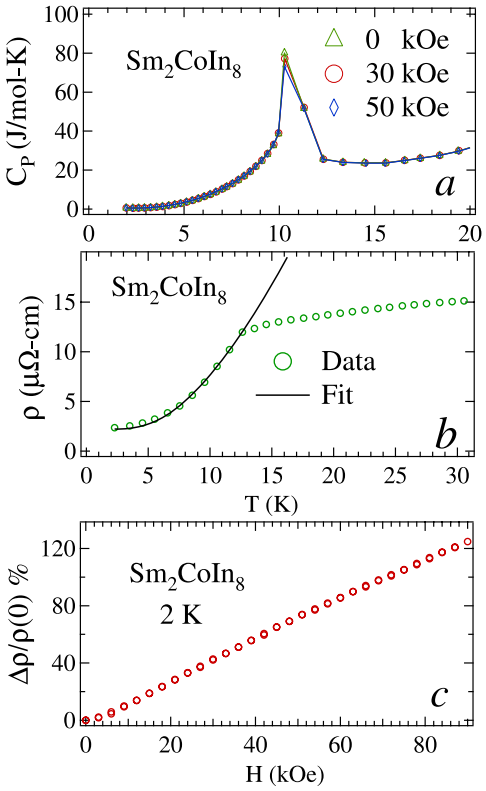

Figure 17. (*a*) Heat capacity of Sm_2CoIn_8 with an applied field of 0, 30, and 50 kOe. The lines joining the data points are guides to the eye. (*b*) Low-temperature resistivity of Sm_2CoIn_8 with a fit in the ordered state to the equation in the text. (*c*) Magnetoresistance for the same at 2 K and up to 90 kOe.

of the compound at 2 K is shown in figure 17(*c*), which shows only a linear increase with the field. This indicates the dominant antiferromagnetic nature of the compound.

The heat capacity behaviour of the compound is shown in figure 17(*a*) for various applied fields. The curves show an anomaly only at the antiferromagnetic transition temperature of the compound (≈12 K) and no anomaly at low temperatures corresponding to the sudden increase in the magnetic susceptibility. The heat capacity in the presence of magnetic field shows no shift in the peak temperature with the field. Even the height of the peak also remains approximately the same. Hence we can assume that there is a strong antiferromagnetic interaction present in the compound.

The upturn of the susceptibility below 5 K and the increase in susceptibility (figure 15(*a*)) with field (from 0.5 to 1 kOe) can be attributed to the presence of a ferromagnetic component due to the incomplete cancellation of the antiferromagnetically ordered spins. The effect of the component is being affected by the temperature similarly to that of the ferromagnetic property of the compound, as is evident from the magnetic isotherms at 2 and 4 K. The virgin curve of the magnetic isotherm at low fields (below 5 kOe) shows nearly zero magnetization (lower inset of figure 16), followed by the linear behaviour. The exact reason for this behaviour is not known, but an initial zero magnetization may be due to the anisotropic behaviour of the ferromagnetic component. The curve undergoes a metamagnetic transition at ≈26 kOe, which may be due to the spin reorientation. The magnetization curve does not follow the

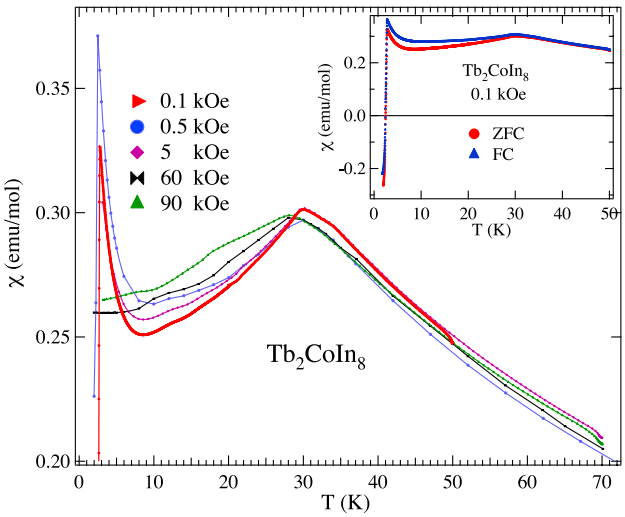

Figure 18. Susceptibility of Tb_2CoIn_8 measured at 0.1, 0.5, 5, 60, and 90 kOe. The inset shows the susceptibility under zero-field-cooled and field-cooled conditions at 0.1 kOe.

same path when the field is decreased, but shows a curve similar to that of a ferromagnetic compound. The magnetoresistance at 2 K increases monotonically with field, as expected for a pure antiferromagnet. The heat capacity at 50 kOe has exactly similar behaviour to that of a zero-field one. Considering these behaviours, we suggest that the metamagnetic transition induces a small ferromagnetic component in the compound which dominates the magnetization behaviour; otherwise the compound has a dominating strong antiferromagnetic behaviour. The hysteretic behaviour in the compound is due to the strong anisotropic behaviour of the Sm^{3+} ions. The Sm^{3+} ions are well known for their strong anisotropic behaviour in the ferromagnetic compounds [26].

3.8. Tb_2CoIn_8

The low-temperature susceptibility versus temperature curve for Tb_2CoIn_8 in various fields (0.5, 5, 60 and 90 kOe) is shown in figure 18. The low-field (0.1 and 0.5 kOe) susceptibility shows two magnetic transitions, at ≈30 and ≈2.5 K, respectively. The transition at 30 K seems to be antiferromagnetic in nature. Below 10 K the low-field susceptibility increases with decrease in temperature and it falls sharply at 2.5 K. To further investigate this behaviour, the susceptibility at 100 Oe was measured under field-cooled (FC) and zero-field-cooled (ZFC) conditions, as shown in the inset of figure 18. The bifurcation of the susceptibility curve under ZFC and FC conditions indicates the presence of a ferromagnetic component below the antiferromagnetically ordered state. The ferromagnetic component may be due to the incomplete cancellation of the antiferromagnetically ordered spins. The susceptibility below 2.5 K falls sharply to a negative region, indicating the possibility of a superconducting transition of the compound. The diamagnetic susceptibility does not saturate down to 1.8 K (the lowest temperature attained by us); hence it is difficult to estimate whether the possibility of superconductivity is a sample property or because of some impurity phase within it. At 5 kOe (figure 18) the transition at 2.5 K disappears but the susceptibility still increases below 10 K. For both 60 and 90 kOe, the susceptibility shows only one magnetic transition (≈30 K) and the peak shifts towards low temperatures. The peak shift towards low temperature indicates

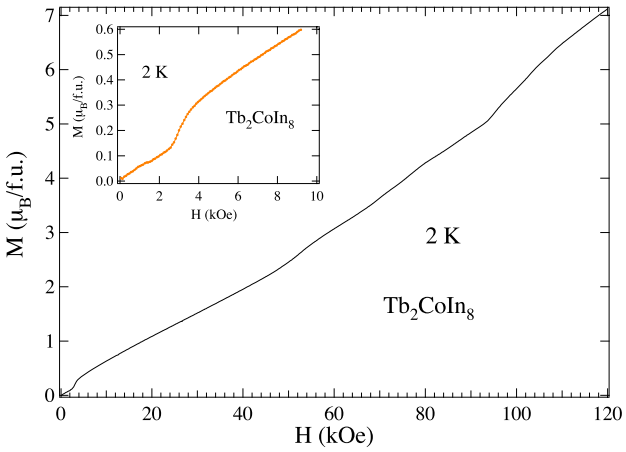

Figure 19. Magnetic isotherm for Tb_2CoIn_8 at 2 K. The inset shows the expanded low-field region to depict the metamagnetic transition.

the antiferromagnetic nature of the magnetic transition at 30 K. The important feature to note is that the susceptibility does not show a smooth variation below the magnetic ordering for all applied fields. In order to further investigate this magnetization behaviour, the magnetization as a function of field was measured at 2 K; this is shown in figure 19. The curve starts with a linear behaviour, but shows the first metamagnetic transition at ≈3 kOe, as shown in the inset of figure 19. As the field is increased further, there are other metamagnetic transition-type discontinuities between 40 and 85 kOe, and the last one is at ≈93 kOe. The first metamagnetic transition at 3 kOe may be due to a spin reorientation and it may be responsible for the second magnetic transition at 2.5 K observed in the low-field magnetic susceptibility. Since only Tb is magnetic in this compound and it is well known for various types of magnetic structure in its compounds, the observed magnetic properties can be attributed to the possibility of complex magnetic structures in this compound. The susceptibility in the paramagnetic region was fitted to the Curie–Weiss law with the values of the parameters in table 3. The values are as expected for the compound.

The specific heat behaviour of the compound in various fields is shown in figure 20(*a*). The curves show an anomaly at the transition temperature of the compound. The transition temperature shifts towards low temperatures with field, indicating the antiferromagnetic behaviour of the compound. Even though the heat capacity curve has a smooth variation below the transition temperature, unlike the magnetic susceptibility, a nearly linear behaviour is observed at low temperatures instead of a T^3 behaviour. To look at the exact nature of the heat capacity curve below T_N, the curve was re-plotted as C/T versus T; this is shown in the inset of figure 20(*a*). The curve shows a broad hump in the temperature range from 5 to 15 K. It is very difficult to make out whether there is any anomaly corresponding to the discontinuity in the magnetic susceptibility at ≈2.5 K. The broad hump might be a characteristic of a Schottky-type anomaly. The calculated magnetic entropy turns out to be ≈21.8 J/mol-K-Tb, a little higher than that expected for a free Tb^{3+} ion (21.3 J/mol-K).

The low-temperature resistivity of the compound is shown in figure 20(*b*). It shows a deviation from the pure metallic behaviour at ≈30 K due to the magnetic ordering of the compound. In the ordered state the resistivity shows nearly linear behaviour above ≈10 K. Below 10 K it deviates from linear behaviour, followed by a strong deviation below ≈3 K in agreement with the magnetization measurement. The magnetoresistance is positive, as shown

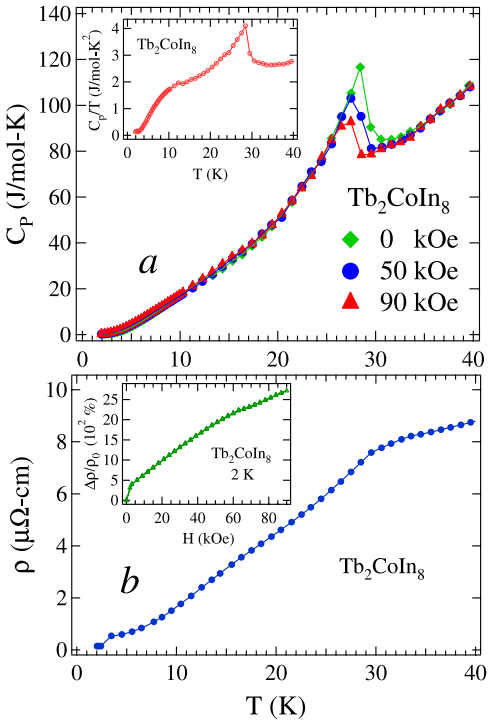

Figure 20. (*a*) Low-temperature heat capacity of Tb_2CoIn_8, with the inset showing the C_P/T versus T plot. (*b*) Low-temperature resistivity of Tb_2CoIn_8, with the inset showing its magnetoresistance at 2 K and up to 90 kOe.

in the inset of figure 20(*b*), indicating the antiferromagnetic behaviour of the compound. The magnetoresistance has a huge value of ≈2700% at 2 K and 90 kOe in this compound. If we exclude the initial jump, which may be due to the superconductivity, then the value is ≈2400%. The highest reported value is 6000%, in $SmAgSb_2$ [27].

3.9. Nd_2CoIn_8

The low-temperature susceptibility of the compound in various fields is shown in figure 21(*a*). The susceptibility at 1 kOe shows an antiferromagnetic ordering at ≈10 K. The peak shifts towards low temperature with increase in the field, as expected for an antiferromagnetic compound. At 80 kOe, there is an appreciable broadening of the peak with an increase in the susceptibility in the antiferromagnetically ordered state, indicating the presence of a ferromagnetic component. For further investigation, the magnetic isotherms of the compound were measured at various temperatures, as shown in figure 21(*c*). The magnetic isotherm at 2 K shows a metamagnetic transition at ≈60 kOe. The sharpness of the metamagnetic transition decreases with increase in temperature with a straight line behaviour in the paramagnetic region (12 K). The decrease in the sharpness is due to the presence of thermal energy to overcome the interaction energy (the energy between the antiferromagnetically ordered moments), and the anisotropy decreases as well. This also causes an increase in the magnetization with temperature in the magnetic isotherms within the ordered state, and in the paramagnetic state it opposes the field-induced ordering; hence the magnetization decreases. The susceptibility of the compound in the paramagnetic state was fitted to the Curie–Weiss law (figure 20(*b*)) with

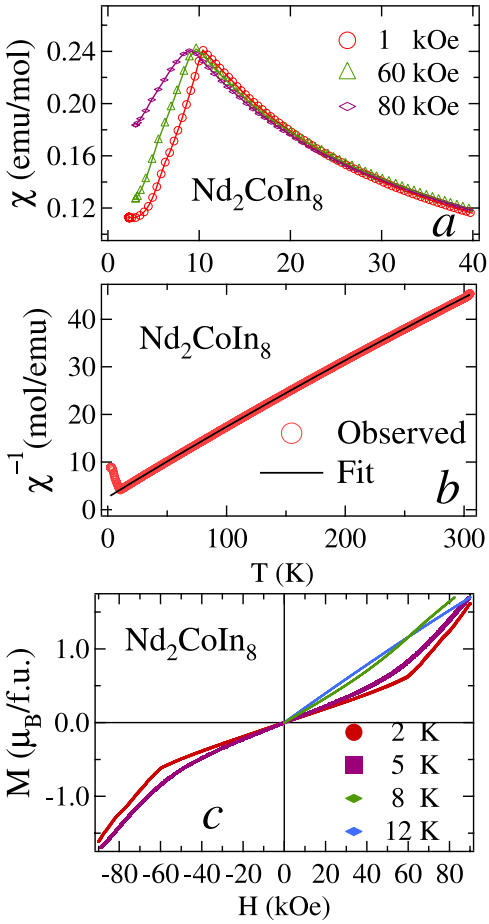

Figure 21. (*a*) Susceptibility of Nd_2CoIn_8 measured at 1, 60, and 80 kOe. (*b*) Inverse susceptibility for the same with the Curie–Weiss fit. (*c*) Magnetic isotherm for the same at 2, 5, 8 and 12 K.

$\mu_{\text{eff}} = 3.6\ \mu_{\text{B}}$ and a paramagnetic Curie temperature of -12 K. The values are within the expectation limits of the compound.

The heat capacity of the compound in various fields is shown in figure 22(*a*). The heat capacity shows an anomaly at the Néel temperature of the compound. The peak height decreases and shifts towards low temperature with field. The peak shift is in agreement with the magnetization behaviour of the compound, and the decrease in the height is due to the additional energy supplied by the field.

The resistivity of the compound shows a metallic behaviour down to the ordering temperature of the compound, below which it decreases due to the disappearance of spin disorder resistivity. The resistivity behaviour in the ordered state was fitted to equation (12) (figure 22(*b*)) with $\rho_0^S = 1.7\ \mu\Omega$ cm, $b = 0.023\ \mu\Omega$ cm K^{-2} and $\Delta = 16$ K. The high value of Δ indicates the high anisotropy associated with the compound. The magnetoresistance at 2 K (figure 22(*c*)) shows a linear increase with field, as expected for an antiferromagnetic compound. Above 80 kOe the curve shows a downward turn, indicating the onset of ferromagnetic behaviour of the compound with field. The curves with increasing and decreasing field coincide with each other (figure 22(*c*)).

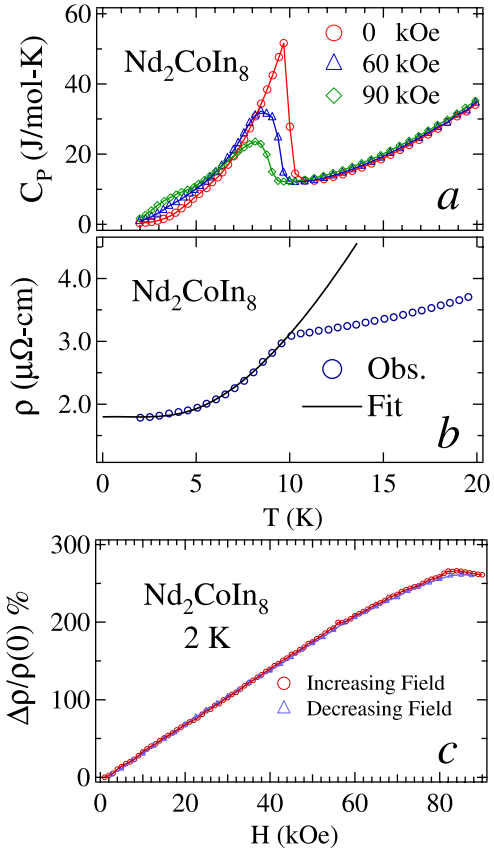

Figure 22. (*a*) Heat capacity of Nd_2CoIn_8 with an applied field of 0, 60, and 90 kOe. The lines joining the data points are guides to eye. (*b*) Low-temperature resistivity of Nd_2CoIn_8 with a fit in the ordered state to the equation in the text. (*c*) Magnetoresistance for the same at 2 K and up to 90 kOe.

4. Conclusion

In conclusion, we have studied the magnetic properties of the R_2CoIn_8 series of compounds. Y_2CoIn_8 shows a Pauli paramagnetic behaviour indicating the non-magnetic behaviour for Co in these compounds. Ce_2CoIn_8 shows a heavy fermion behaviour at low temperatures and a Kondo effect at high temperatures. Pr_2CoIn_8 shows a crystal field effect at low temperatures. The other magnetic rare earths (R = Sm, Nd, Gd, Tb, Dy and Ho) show antiferromagnetic ordering at low temperatures with T_N = 12, 10, 33.5, 30, 17.4 and 7.6 K, respectively. Dy_2CoIn_8 shows spin reorientation at low temperature and metamagnetic transitions in the magnetic isotherms. It shows a field-induced ferromagnetic state at 2 K and above ≈82 kOe. Ho_2CoIn_8 and Nd_2CoIn_8 also show metamagnetic transitions and a field-induced ferromagnetic transition at 2 K and above ≈54 and 85 kOe respectively. Gd_2CoIn_8 is a strong antiferromagnet. Sm_2CoIn_8 shows a dominating antiferromagnetic behaviour with a ferromagnetic component at low temperatures. The hysteresis curve above the metamagnetic transition behaves as an anisotropic ferromagnet even if the field is reduced to zero. Tb_2CoIn_8 shows a ferromagnetic component at low temperatures with the possibility of superconducting behaviour below

2.5 K. The compound also shows metamagnetic transitions in the magnetic isotherm and the possibility of complicated magnetic structure below the transition temperature.

References

[1] Kalychak Ya M, Zeremba V I, Baranyak V M, Bruskov V A and Zavalij P Yu 1989 *Izv. Acad. Nauk SSSR Met.* **1** 209
[2] Kalychak Ya M 1999 *J. Alloys Compounds* **291** 80
[3] Hegger H, Petrovic C, Moshopolou E G, Hundley M F, Sarrao J L, Fisk Z and Thompson J D 2000 *Phys. Rev. Lett.* **84** 4986
[4] Thompson J D *et al* 2001 *J. Magn. Magn. Mater.* **226** 5
[5] Nicklas M, Shidorov V A, Borges H A, Pagliuso P G, Petrovic C, Fisk Z, Sarrao J L and Thompson J D 2003 *Phys. Rev.* B **67** 020506
[6] Petrovic C, Movshovich R, Jaime M, Pagliuso P G, Hundley M F, Sarrao J L, Fisk Z and Thompson J D 2001 *Europhys. Lett.* **53** 354
[7] Petrovic C, Pagliuso P G, Hundley M F, Movshovich R, Sarrao J L, Thompson J D, Fisk Z and Monthoux P 2001 *J. Phys.: Condens. Matter* **13** L337
[8] Chen G, Ohara S, Hedo M, Uwatoko Y, Saito K, Sorai M and Sakamoto I 2002 *J. Phys. Soc. Japan* **71** 2836
[9] Chen G, Ohara S, Hedo M, Uwatoko Y and Sakamoto I 2001 *J. Phys.: Condens. Matter* **15** S2175
[10] Joshi D A, Tomy C V, Nagrajan R, Nirmala R and Malik S K 2005 *J. Appl. Phys.* **97** 10A920
[11] Buschow K H J 1969 *J. Chem. Phys.* **50** 137
[12] Nieuwenhuys G J, Maclaughlin D E and Bernal O O 2004 *Phys. Rev.* B **69** 214415
[13] Adroja D T and Malik S K 1992 *Phys. Rev.* B **45** 779 and references therein
[14] Rajan V T 1983 *Phys. Rev. Lett.* **51** 803
[15] Trainor R J, Broadsky M B and Culbert H V 2000 *Phys. Rev. Lett.* **34** 1019
[16] Mathur N D *et al* 1998 *Nature* **394** 39
[17] Kondo J 1964 *Prog. Theor. Phys. Japan* **32** 37
[18] Schlottmann P 1989 *Phys. Rep.* **181** 1
[19] Menon L and Malik S K 1995 *Phys. Rev.* B **51** 5858
[20] Mrachkow J, Leyarovaski E, Gilewski A, Mydlarz T and Iliev N 1988 *Physica* B **154** 66
[21] Bleaney B 1963 *Proc. R. Soc.* A **276** 19
[22] Bouvier M, Lethuillier P and Schmitt D 1991 *Phys. Rev.* B **43** 13137
[23] de Wijn H W, van Diepen A M and Buschow K H J 1970 *Phys. Rev.* B **1** 4203
[24] Fontes M B, Trochez J C, Giordanengo B, Budko S L, Sanchez D R and Saitovitch E M B 1999 *Phys. Rev.* B **60** 6781
[25] Hamakar H C, Wolf L D, Mackey H B, Fisk Z and Maple M B 1979 *Solid State Commun.* **32** 289
[26] Buschow K H J 1991 *Rep. Prog. Phys.* **54** 1123
[27] Mayors K D, Budko S L, Fisher I R, Islam Z, Kleinke H, Lacerda A H and Canfield P C 1999 *J. Magn. Magn. Mater.* **205** 27